Brain criticality characterizes abnormal neural dynamics and metabolism in disorder of consciousness

Qianqian Ge[1,†], Yumeng Xin[2,3,†], Chen He[1], Shuai Han[1], Xiaoli Geng[1], Xueling Chen[1], Shan Yu[4,5,6,7], Jianghong He[1,*], Ning Liu[2,3,*], Long Xu[1,*]

Supplementary Text

Supplementary Methods

Parameter estimation for the Ising model

Traditionally, Ising model parameters *h* and *J* are estimated using maximum likelihood estimation (MLE). In this framework, the optimal parameter set (***h***, ***J***) maximizes the probability of the observed data under the model:

$$(\boldsymbol{h},\boldsymbol{J}) = \underset{\mathbf{h},\mathbf{J}}{\operatorname{argmax}}\, \mathcal{L}(\boldsymbol{h},\boldsymbol{J}), \tag{1}$$

where the likelihood function $\mathcal{L}(\boldsymbol{h}, \boldsymbol{J})$ is defined as:

$$\mathcal{L}(\boldsymbol{h},\boldsymbol{J}) = \prod_{t=1}^{t_{max}} \mathrm{P}(\boldsymbol{\sigma}(t) \mid \boldsymbol{h},\boldsymbol{J}), \tag{2}$$

where P is the Boltzmann distribution function representing the probability of observing a given spin configuration σ:

$$\mathrm{P}(\boldsymbol{\sigma}(t) \mid \boldsymbol{h},\boldsymbol{J}) = \frac{e^{-E(\boldsymbol{\sigma}|\boldsymbol{h},\boldsymbol{J})}}{\sum_{\{\boldsymbol{\sigma}'\}} e^{-E(\boldsymbol{\sigma}'|\boldsymbol{h},\boldsymbol{J})}}. \tag{3}$$

The gradient descent method was used to optimize *h* and *J*:

$$h_i^{new} = h_i^{old} + \alpha(\langle\sigma_i\rangle_{emprical} - \langle\sigma_i\rangle_{model}), \tag{4}$$

$$J_{ij}^{new} = J_{ij}^{old} + \alpha(\langle\sigma_i\sigma_j\rangle_{emprical} - \langle\sigma_i\sigma_j\rangle_{model}), \tag{5}$$

where old and new denote parameter values before and after the update, and α is the learning rate. However, for large systems, traditional MLE becomes computationally challenging. Accordingly, following previous studies, we employed pseudo-likelihood estimation,[1-3] a mean-field approximation that approaches the true likelihood as the number of time points increases:

$$\mathcal{L}(\boldsymbol{h},\boldsymbol{J}) = \prod_{t=1}^{t_{max}} \mathrm{P}(\boldsymbol{\sigma}(t)|\boldsymbol{h},\boldsymbol{J}) \approx \prod_{t=1}^{t_{max}} \prod_{i=1}^{N} \tilde{\mathrm{P}}\,(\sigma_i(t)|\boldsymbol{h},\boldsymbol{J},\boldsymbol{\sigma}_{/i}(t)), \tag{6}$$

where $\tilde{\mathrm{P}}\,(\sigma_i(t)|\boldsymbol{h},\boldsymbol{J},\boldsymbol{\sigma}_{/i}(t))$ is the modeled probability of a given spin, conditional on the states of all others:

$$\tilde{\mathrm{P}}\,(\sigma_i(t)|\boldsymbol{h},\boldsymbol{J},\boldsymbol{\sigma}_{/i}(t)) = \frac{exp[h_i\sigma_i + \sum_{\mathrm{j}\,=\,1,\,\mathrm{j}\,\neq\,\mathrm{i}}^{N} J_{ij}\sigma_i\sigma_j(t)]}{\sum_{\sigma_i'\,=\,-1,+1} exp[h_i\sigma_i' + \sum_{\mathrm{j}\,=\,1,\,\mathrm{j}\,\neq\,\mathrm{i}}^{N} J_{ij}\sigma_i'\sigma_j(t)]}. \tag{7}$$

With this approximation, the gradient ascent update becomes:

$$h_i^{new} = h_i^{old} + \alpha(\langle\sigma_i\rangle_{emprical} - \langle\sigma_i\rangle_{\tilde{\mathrm{P}}}), \tag{8}$$

$$J_{ij}^{new} = J_{ij}^{old} + \alpha(\langle\sigma_i\sigma_j\rangle_{emprical} - \langle\sigma_i\sigma_j\rangle_{\tilde{\mathrm{P}}}), \tag{9}$$

where $\langle\sigma_i\rangle_{\tilde{\mathrm{P}}}$ and $\langle\sigma_i\sigma_j\rangle_{\tilde{\mathrm{P}}}$ are the one- and two-point correlation functions with respect to the model distribution,

$$\langle\sigma_i\rangle_{\tilde{\mathrm{P}}} = \frac{1}{t_{max}}\sum_{t=1}^{t_{max}} tanh\left[h_i + \sum_{\mathrm{j'}\,=\,1,\,\mathrm{j'}\,\neq\,\mathrm{i}}^{N} J_{ij'}\,\sigma_{j'}(t)\right], \tag{10}$$

$$\langle\sigma_i\sigma_j\rangle_{\tilde{\mathrm{P}}} = \frac{1}{t_{max}}\sum_{t=1}^{t_{max}} \sigma_j(t)tanh\left[h_i + \sum_{\mathrm{j'}\,=\,1,\,\mathrm{j'}\,\neq\,\mathrm{i}}^{N} J_{ij'}\,\sigma_{j'}(t)\right]. \tag{11}$$

Supplementary Results

Differences in PET values between UWS and MCS

We compared metabolic activity between UWS and MCS patients using PET imaging. The difference in whole-brain metabolic values between groups were marginally significant, with MCS patients showing a tendency toward higher metabolic activity (Supplementary Fig. 3A, $t(24) = 1.90$, $P = 0.069$). Regional analyses revealed consistently higher metabolic values in MCS patients across most brain regions (more than 100 regions reached statistical significance before p-value correction), though these differences did not reach statistical significance after multiple- comparison correction (Supplementary Fig. 3B).

Diagnosis and prognosis of patients with DoC by using PET values

We further evaluated whether regional PET values can be used for both diagnostic classification (MCS vs. UWS) and prognostic prediction (Supplementary Fig. 3D&F). We found that SVM classifiers achieved moderate accuracy for diagnosis (accuracy = 61.54%, AUC = 0.57) and prognosis (accuracy = 52.00%, AUC = 0.39). Notably, these results were substantially lower than those achieved with critical metrics (Fig. 5).

Supplementary Figures

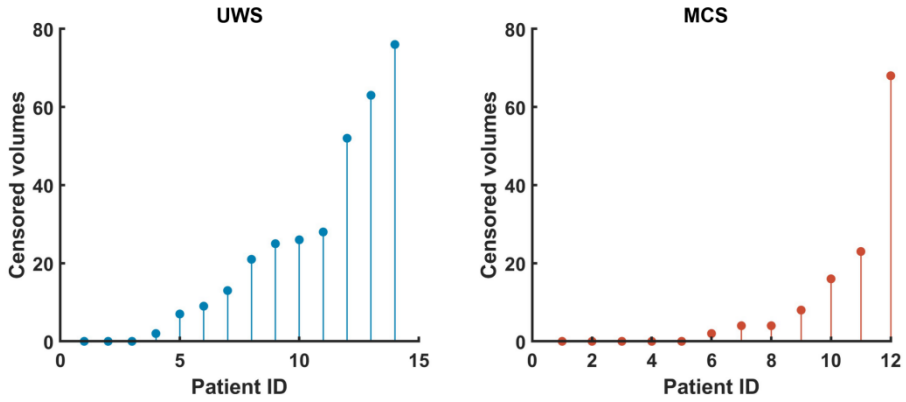

Fig. 1 Number of volumes censored due to head motion and outliers. Each point represents one participant. The left panel shows UWS patients and the right panel shows MCS patients. Participants are ranked according to the number of censored volumes.

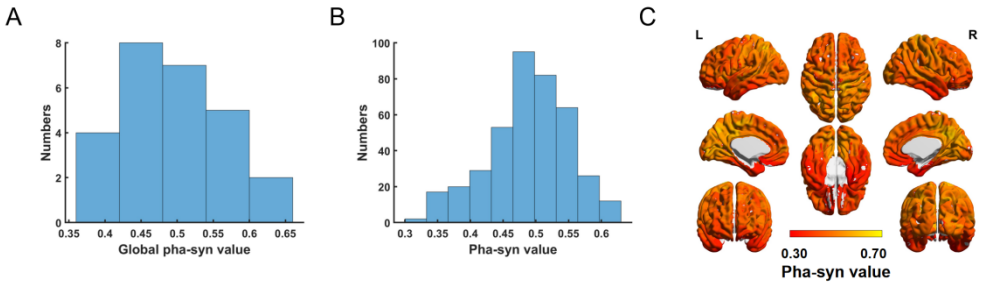

Fig. 2 Distribution of pha-syn values. (A) Distribution of global synchrony values across the 26 DoC patients. (B) Distribution of the pha-syn values of the 400 ROIs (averaged across patients), along with the corresponding brain map (C).

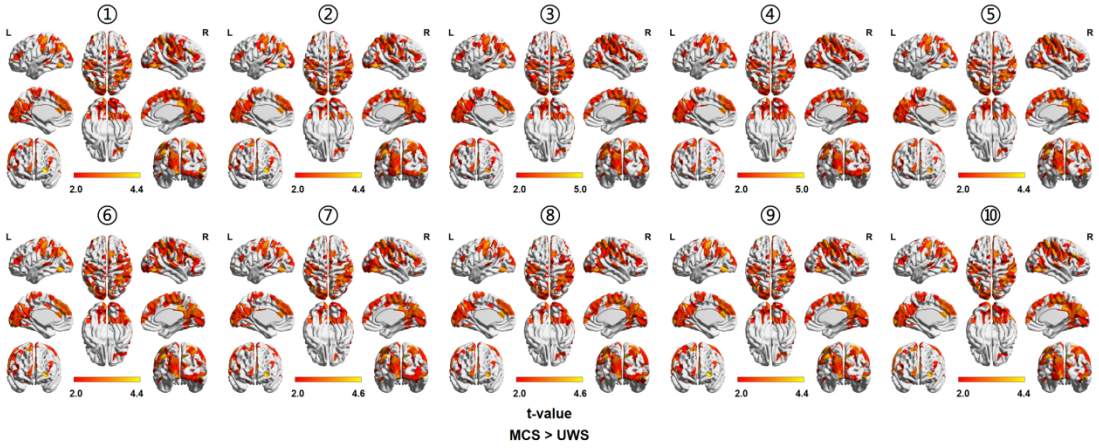

Fig. 3 Regional phase synchrony differences between UWS and MCS under voxel subsampling. For each brain region, only half of the voxels were randomly sampled to compute phase synchrony. The figure shows the results across 10 independent random sampling iterations. Regions showing significant group differences are highlighted in red ($P < 0.05$, uncorrected). The overall spatial pattern of group differences remained largely stable across samplings.

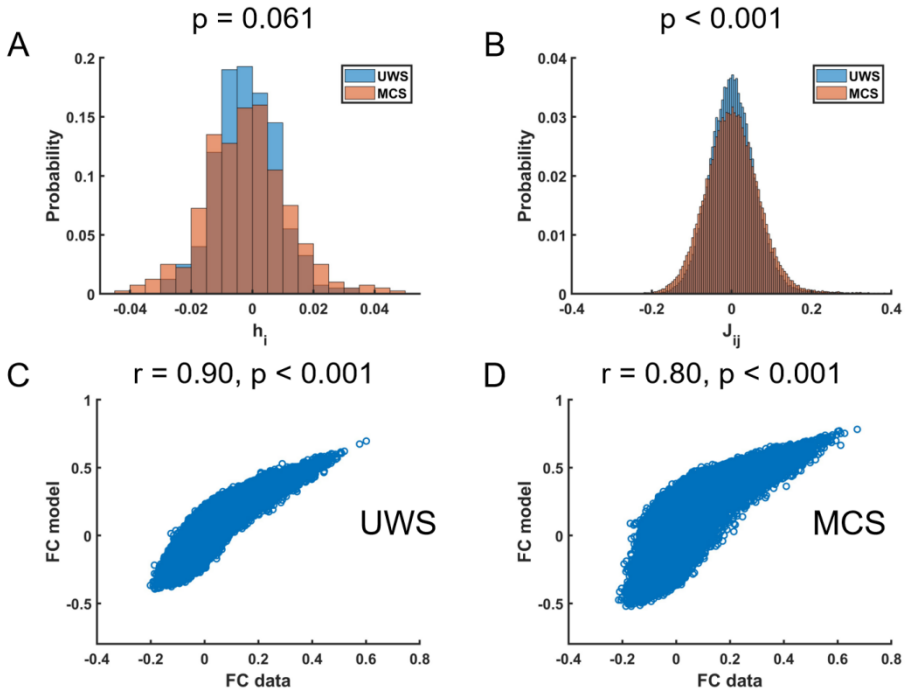

Fig. 4 Ising model parameters and modeled functional connectivity. (A-B) Distributions of h_i and J_{ij} for UWS and MCS, respectively. (C-D) Correlations between the functional connectivity of empirical and simulated data for the UWS and MCS groups, respectively.

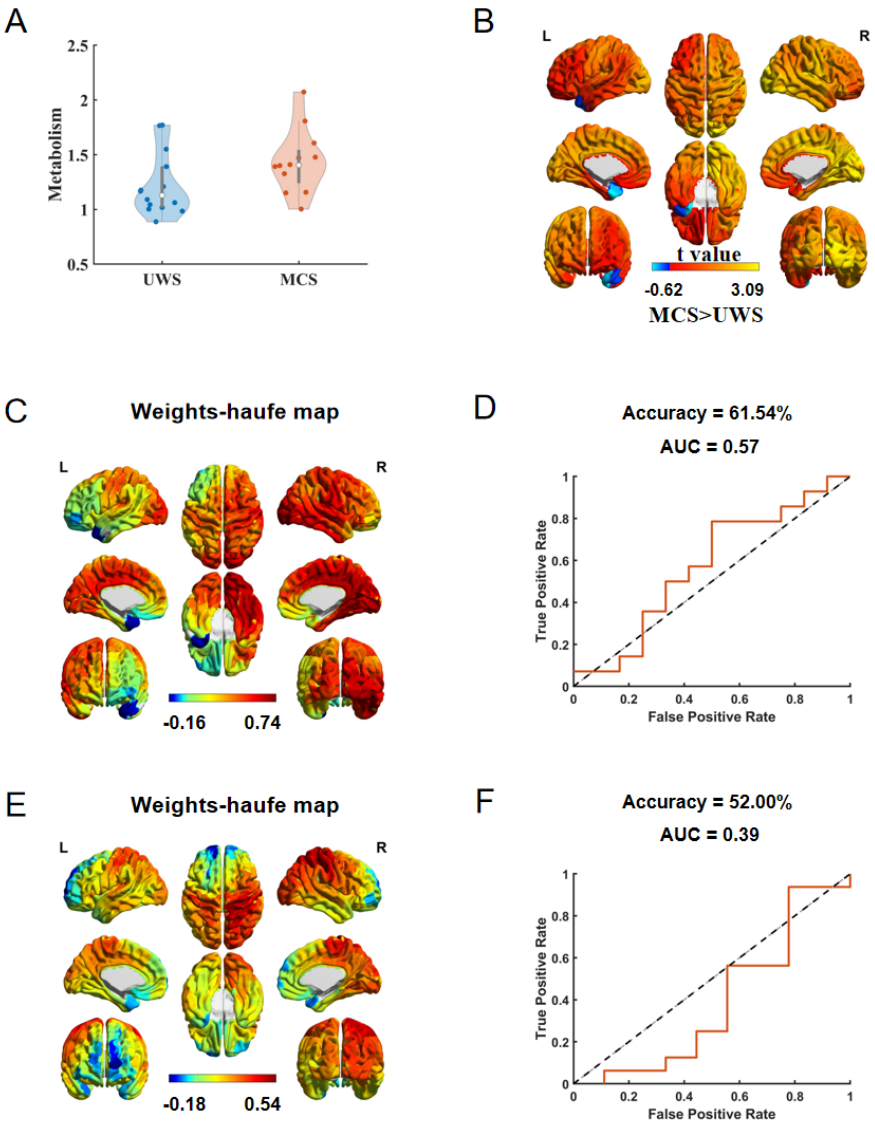

Fig. 5 PET analysis results. (A) Statistical comparison of whole-brain PET values between MCS and UWS. (B) Regional t-statistic map illustrating differences in PET values between MCS and UWS. (C) Weight map showing the contribution of each region to the diagnostic classification based on regional metabolism; (D) Left: accuracy and ROC curve for the diagnostic task using the regional metabolism; Right: Diagnostic performance based on the top features with the highest weights. (E-F) As in panel (C-D), but for the prognostic task.

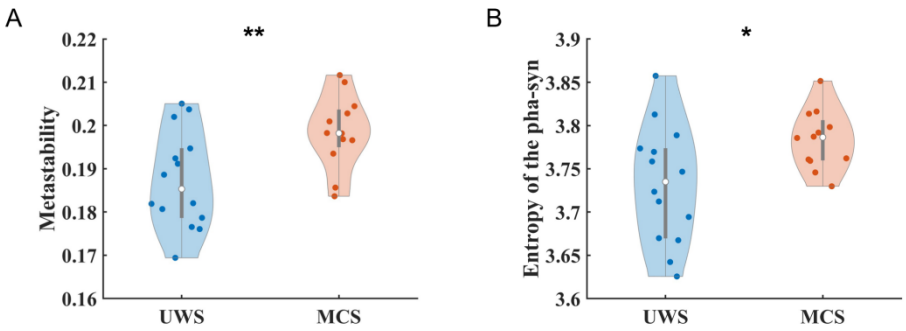

Fig. 6 Global dynamical metrics. (A) Global metastability and (B) entropy of the pha-syn statistics. ** indicates $p < 0.01$, * indicates $p < 0.05$.

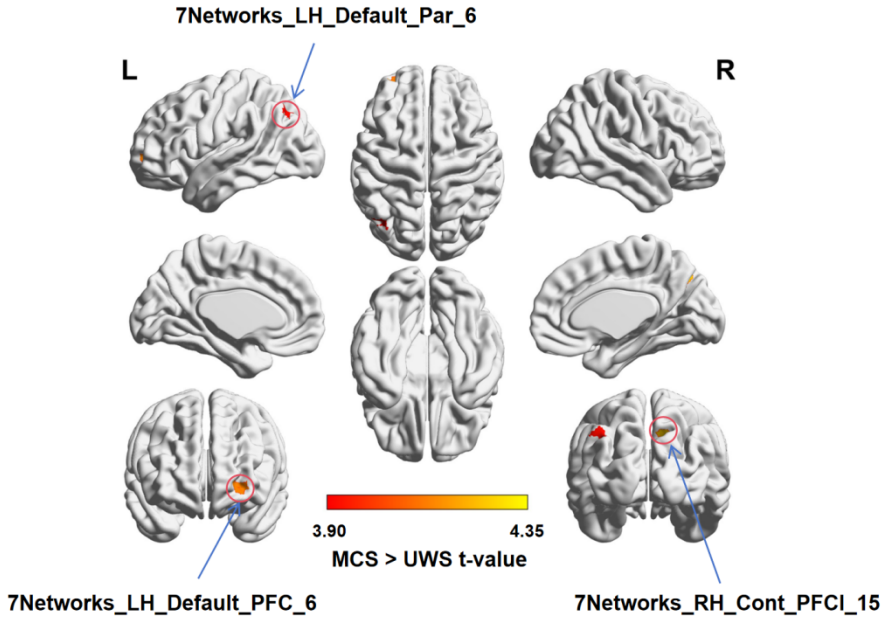

Fig. 7 Regional phase synchronization (pha-syn) analysis results after multiple-comparison correction. Significant regions are labeled and indicated by arrows.

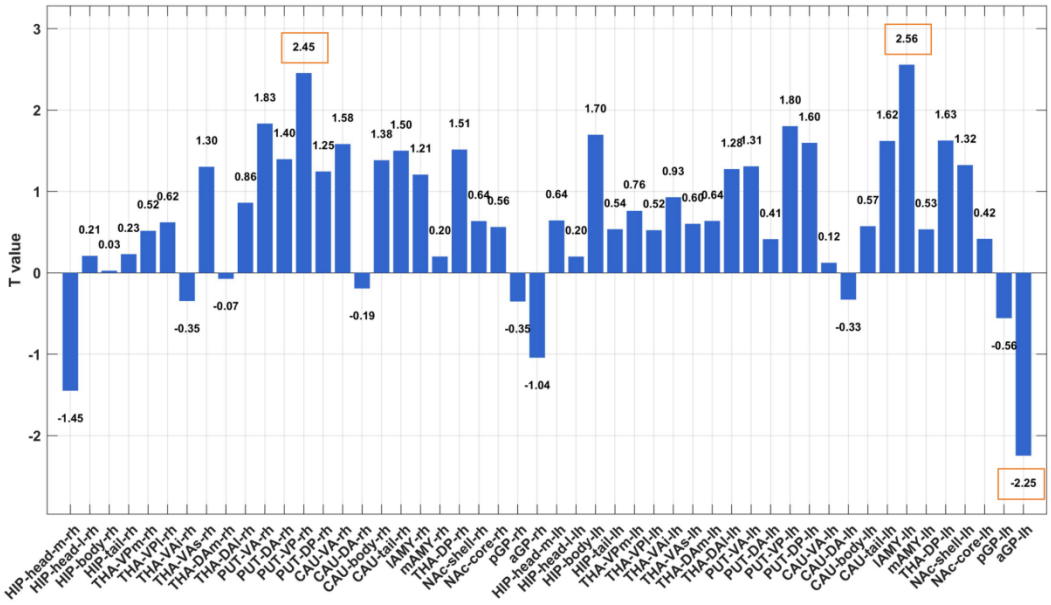

Fig. 8 Phase synchrony statistics in subcortical areas. T values are shown above or below each bar. Regions reaching statistical significance are highlighted with red boxes.

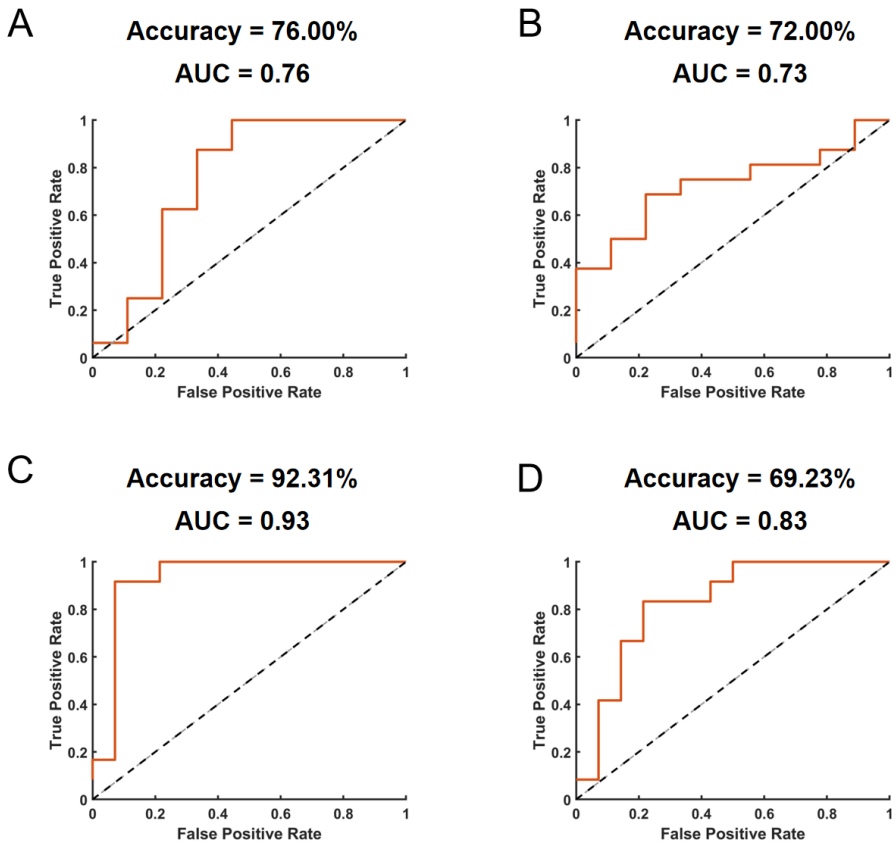

Fig. 9 Cross-task classification performance. (A) Original performance of the prognostic classifier. (B) Performance of the diagnostic classifier when applied to the prognostic task. (C) Original performance of the diagnostic classifier. (D) Performance of the prognostic classifier when applied to the diagnostic task.

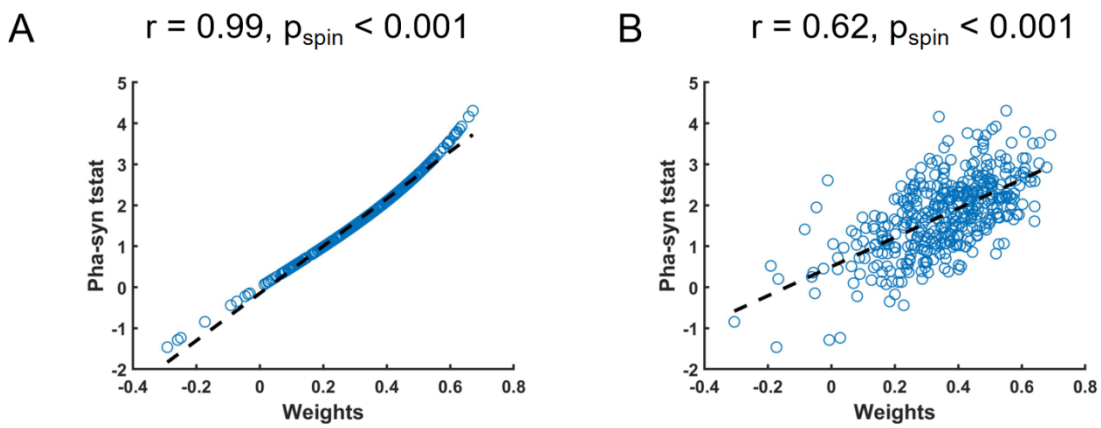

Fig. 10 Correlations between the phase synchronization t-statistic map and SVM weights (A) Correlations for the diagnostic task. (B) Correlations for the prognostic task.

References

1 Ruffini, G. *et al.* LSD-induced increase of Ising temperature and algorithmic complexity of brain dynamics. *Plos Computational Biology* **19**, doi:10.1371/journal.pcbi.1010811 (2023).

2 Ponce-Alvarez, A. *et al.* Macroscopic Quantities of Collective Brain Activity during Wakefulness and Anesthesia. *Cerebral Cortex* **32**, 298-311, doi:10.1093/cercor/bhab209 (2022).

3 Ezaki, T., Watanabe, T., Ohzeki, M. & Masuda, N. Energy landscape analysis of neuroimaging data. *Philos T R Soc A* **375**, doi:10.1098/rsta.2016.0287 (2017).